applied optics

Adjustable flexure mount to compensate for deformation of an optic surface

ZHOU FENG,[1] YU JIE,[1,2] WANG LI-PING,[1] LI YUAN-MING,[1] ZHANG HAI-TAO,[1,2] MAN QUAN,[1] LI QIANG,[1] BI RAN,[1] WANG HUI,[1,2,*] AND JIN CHUN-SHUI[1]

[1]State Key Laboratory of Applied Optics, Changchun Institute of Optics, Fine Mechanics and Physics, Chinese Academy of Sciences, Changchun, Jilin 130033, China
[2]University of Chinese Academy of Sciences, Beijing 100049, China
*Corresponding author: wanghui@ciomp.ac.cn

Received 29 August 2019; revised 1 November 2019; accepted 1 November 2019; posted 1 November 2019 (Doc. ID 376669); published 22 November 2019

An adjustable mounting structure is proposed to compensate for surface deformation of a mirror caused by the assembly process. The mount adopts a six-point support based on the kinematic mount principle. Three of the support points are adjustable, and they are moved along the axial direction by actuators. Surface deformation is expressed by Zernike coefficients in this paper, and a sensitivity matrix of the surface deformation is established by varying the unit displacement of each adjustment support point and getting the corresponding Zernike coefficient changes. The surface deformation is measured, and the compensation adjustment of each adjustable support point is then obtained by anti-sensitivity calculation. Finally, the feasibility of present support structure design and surface figure compensating method are verified by experiments. The experimental results show that the present structure and method could significantly reduce the surface deformation caused by the assembly process. The surface deformation is 4.6 nm RMS after assembly and it is decreased to 1.3 nm RMS after four iterations of compensation, which is close to the 1.1 nm RMS after optical polishing.

https://doi.org/10.1364/AO.58.009370

1. INTRODUCTION

The mount of an optical element is an important part of a high-performance optical system. A well-designed mount is able to reduce the inner stress mainly introduced during assembly, reduce the thermal deformation effect, and maintain the assembly accuracy under vibration [1]. Kinematic coupling is a classical optic mounting mechanism that theoretically meets all these requirements. A kinematic mount design follows the principle of exact constraint, which means the mounting structure constrains exactly six degrees of freedom (DOFs) of the optical element without redundancy [2]. Ideally, the design performs excellently in terms of repeatability and reproducibility of the optic surface, thermal stability of the optics, and the stiffness of the mounting structure [3–5]. However, kinematic coupling requires a completely frictionless and ideal point contact, which is difficult to achieve in practice. Instead, semi-kinematic coupling, typically adopting flexure, has been widely used in precision optical application. The use of flexure is effective in releasing or constraining a specific DOF and is free from friction and hysteresis [6]. A semi-kinematic mounting based on flexure often has three equally spaced bipod flexures or blade structures distributed around the optical element. Each flexure of the semi-kinematic mounting constrains two DOFs, for a total of six constraints [7]. This provides high stiffness for the optical components. In addition to providing constraints, the use of flexure produces other local DOFs. Flexure thus allows elastic motion in these DOFs, reduces the internal stress of the optical element, and ensures that the optical element remains in a relatively "relaxed" state. However, factors such as the manufacturing tolerances, mount assembly, and fastening process limit or degrade the performance of the semi-kinematic mount; i.e., there exist relatively large astigmatism, trefoil, spherical, and other aberrations. Indeed, astigmatism and trefoil are usually too large and require correction in precision application [8–10].

We developed an adjustable flexure mount as an optic mount to achieve ultra-high optical precision that is close to that of ideal kinematic coupling. This paper will give an introduction for the principle of the mount design and a method of compensating for the surface figure. Then the surface compensation sensitivity matrix is established through finite element simulation. Finally, the feasibility of using the adjustable flexure mount to compensate for the deformation of the optic surface introduced by the supporting mount is experimentally verified.

2. THEORETICAL ANALYSIS

A. Principles of the Adjustable Flexure Mount

The principles of the kinematic mounting of an optical element are shown in Fig. 1(a). There are two Cartesian coordinate systems, namely, the global coordinate system of the optic {G} (x–y–z) and the local coordinate system of the single mount point {L} (r–t–z). The optic as a rigid object usually has three translations (Tx, Ty, Tz) and three rotations (Rx, Ry, Rz) as DOFs in coordinate system {G}. a_i $(i = 1, 2, 3)$ represents the main mounting points, with each point providing two constraints (Tz, Tt) and four DOFs (Tr, Rr, Rz, Rt) in coordinate system {L}. An ideal kinematic mount with three mounting points is then supposed to constrain exactly six DOFs (Tx, Ty, Tz, Rx, Ry, Rz) in coordinate system {G} without redundancy.

We propose an adjustable flexure mount to improve the performance of the optic mount, especially in terms of achieving high optical precision close to that of ideal kinematic coupling. The principles of our adjustable flexure mount of optics are shown in Fig. 1(b). a_i $(i = 1, 2, 3)$ denotes the main mounting points, with each point providing one constraint (Tz) and five DOFs (Tr, Tt, Rr, Rz, Rt) in coordinate system {L}. b_i $(i = 1, 2, 3)$ denotes the assisting mounting points, which are adjustable in the z direction. Each assisting mounting point provides one constraint (Tt), one adjustable constraint (ATZ), and four DOFs (Tr, Rr, Rz, Rt) in coordinate system {L}. In this case, as viewed in coordinate system {G}, the optic is steadily supported with six mounting points that provide six constraints (Tx, Ty, Tz, Rx, Ry, Rz). Meanwhile, with careful adjustment, the additional constraint (ATZ) is able to compensate for the deformation of the optic surface, especially astigmatism and trefoil.

B. Mechanical Design

An adjustable flexure mount is designed based on the principles described in subsection A, and the schematic drawing is shown in Fig. 2(a). Six flexure structures are equally spaced around the optical element. The main mount, as shown in Fig. 2(b), was realized by a flexural hinge structure, which provides one constraint (Tz) as explained in subsection A. As shown in Fig. 2(c), the adjustable flexure mount is realized by a parallel distribution blade structure, which could provide one constraint (Tt). Two disc springs are placed between the adjustable flexure mount and base, and the adjustable flexure mount could rise or fall by adjusting the screw, causing the deformation of the blade structure and then providing the optical element one adjustable force along the z direction. Therefore, the adjustable flexure mount provides one constraint (Tt) and one adjustable constraint (ATZ).

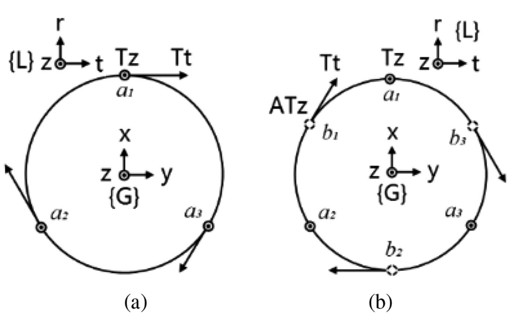

Fig. 1. Principles of the (a) kinematic mount and (b) adjustable flexure mount.

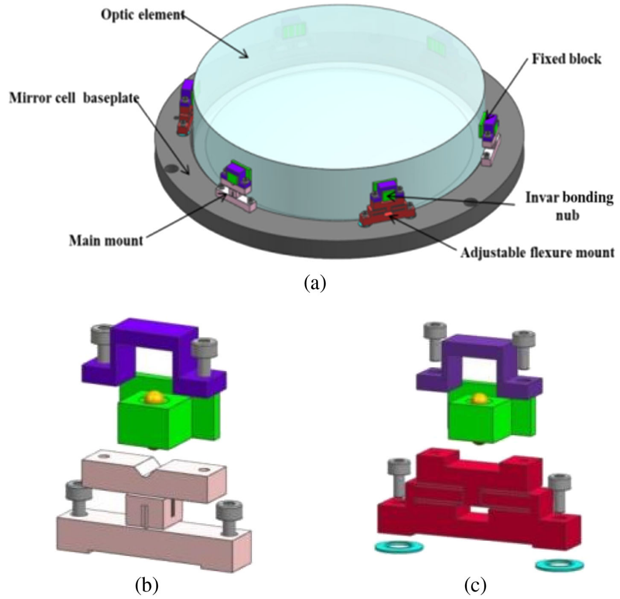

Fig. 2. (a) Mount structure of the optical element, (b) structure of the main mount, (c) structure of the adjustable flexure mount.

C. Establishment of the Strategy to Compensate for the Surface Deformation

The relationship between surface deformation and the adjustment of the adjustable flexure mount can be expressed as $W(x)$, where W is the surface deformation and x is the adjustment. The Taylor expansion of $W(x)$ can be expressed as

$$W(x + \Delta x) = W(x) + A\Delta x + O(\Delta x^2). \tag{1}$$

Generally, the adjustment of an adjustable flexure mount is smaller than dozens of micrometers, and the last term in Eq. (1) is very small and can be ignored. In this case, $W(x)$ is nearly linear to the adjustment.

Zernike polynomials are widely used as basic functions to describe the figure of the optic surface or the deformation of an optic surface [11–19]. The deformation due to the kinematic mount is hypothesized to be an expansion of the first n fringe Zernike polynomials in the form

$$W_K(\rho, \theta) = \sum_{i=4}^{n} a_i^K Z_i(\rho, \theta), \tag{2}$$

where ρ and θ are normalized in polar coordinates, $Zi(\rho, \theta)$ is the ith Zernike polynomial, and a_i^K is the corresponding Zernike coefficient. Terms of piston, tilt, and power ($Z1$ to $Z4$) are neglected, as they are not in the scope of the present application. Similar to Eq. (2), the deformation due to the adjustable flexure mount can be represented as

$$W_{\mathrm{AT}}(\rho, \theta) = \sum_{i=4}^{n} a_i^{\mathrm{AT}} Z_i(\rho, \theta), \tag{3}$$

where a_i^{AT} is the corresponding Zernike coefficient of the deformation. Combining Eq. (2) with Eq. (3), the difference in the mount-introduced deformation between the adjustable flexure mount and ideal kinematic mount is expressed as

$$\Delta W(\rho,\theta) = W_{AT}(\rho,\theta) - W_K(\rho,\theta)$$

$$= \sum_{i=4}^{n} \Delta a_i Z_i(\rho,\theta), \tag{4}$$

where Δa_i is the ith change of the Zernike coefficient between the adjustable flexure mount and the ideal kinematic mount, which can form a column vector **a** as follows:

$$a = [\Delta a_4, \Delta a_5, \cdots, \Delta a_n]^T, \tag{5}$$

where n is the number of Zernike polynomials used to express the surface deformation. The surface deformation is mainly caused by the difference between the adjustable flexure mount and the ideal kinematic mount. Moreover, the main error sources are factors such as manufacturing tolerances, mount assembly, and fastening process, which will degrade the performance of the semi-kinematic mount, i.e., there will be relatively large astigmatism and trefoil aberrations.

In the case of the adjustable flexure mount, the adjustable DOF ATZs are used to compensate for the surface deformation, especially astigmatism and trefoil. The adjustable DOF ATZs form a column vector x as follows:

$$x = [\mathrm{ATZ}_1, \cdots, \mathrm{ATZ}_m]^T, \tag{6}$$

where m is the number of adjustable DOF ATZs. This number is usually an integral multiple of 3 with a minimum value of 3.

Each ATZ driven by an actuator deforms the surface of the optics, and the deformation can be considered the ATZ's influencing functions (IFs). Each ATZ and the deformation response of one unit $\mathrm{ATZ}_i (1 \le i \le m)$ are expressed by $\Delta a_{\mathrm{ATZ}i}$, as follows:

$$\mathrm{ATZ}_1 \to \Delta a_{\mathrm{ATZ}1} = \left[\Delta a_4^{\mathrm{ATZ}1}, \Delta a_5^{\mathrm{ATZ}1}, \cdots, \Delta a_n^{\mathrm{ATZ}1}\right]^T \cdots$$

$$\mathrm{ATZ}_m \to \Delta a_{\mathrm{ATZ}m} = \left[\Delta a_4^{\mathrm{ATZ}m}, \Delta a_5^{\mathrm{ATZ}m}, \cdots, \Delta a_n^{\mathrm{ATZ}m}\right]^T, \tag{7}$$

where m is the number of adjustable DOF ATZs and n is the number of Zernike polynomials used to express the surface deformation. All influencing functions a_{ATZ} then constitute the matrix

$$A = [\Delta a_{\mathrm{ATZ}1}, \cdots, \Delta a_{\mathrm{ATZ}m}], \tag{8}$$

where A is an $(n-3) \times m$ matrix, named the sensitivity matrix. If the deformation response is assumed linear with a change in ATZ_i, we have

$$a = A\Delta x, \tag{9}$$

where Δx is the compensation of each adjustable DOF ATZ. Equation (9) will be an overdetermined system of linear equations if there are more equations than unknowns, and Δx can be calculated by the following anti-sensitive process:

$$\Delta x = (A^T A)^{-1} A^T a. \tag{10}$$

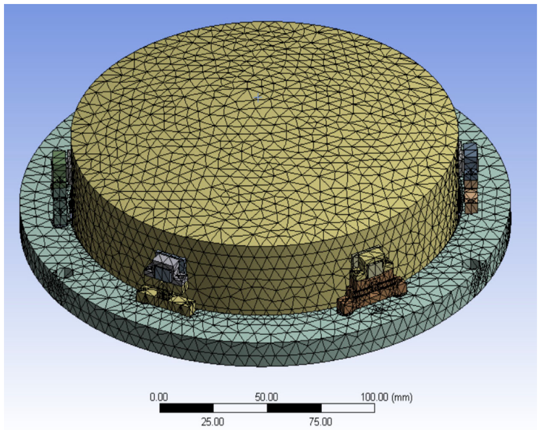

Fig. 3. FEA model.

3. ESTABLISHING SENSITIVITY MATRIX A

Finite element analysis (FEA) is adopted to build matrix A in Eq. (8). A model of the novel semi-kinematic mount is built in FEA software as shown in Fig. 3. The material of the optic is ultra-low expansion glass (ULE), while the material of the mounting flexure and base is Invar 36. The mounts and mirror are bonded with epoxy, and the thickness of the adhesive layer is 0.1 mm. The detailed FEA parameters are listed in Table 1.

The optical axis of the mirror is in vertical attitude, and the surface is upward. This attitude remains the same during figure measurement for optical polishing, for assembly, and for adjustment. The measurement mount during optical polishing is a kinematic mount, and the adjustable flexure mount used in the assembly and adjustment process is a semi-kinematic mount. These mounts can achieve a completely consistent attitude and stress state. Therefore, the additional effect of gravity is not considered in the simulation.

In the simulation, an axial displacement of −20 μm is applied to adjust the three support points in turn, and the displacements of the nodes and elements of the model are then calculated. We select surface nodes as the simulation output. The first 36 terms of the Zernike polynomials are used to represent surface deformation, and the displacement of surface nodes is fitted. In this process, three sets of Zernike polynomials are obtained to build influence functions.

The influence functions have also been built by experiment. Three support points are adjusted with axial displacement of −20 μm in turn, and the surface deformation is measured by interferometer and is represented by the first 36 terms of the Zernike polynomials. The experimental and numerical results of the IFs are shown in Fig. 4.

It is clear that astigmatism ($Z5$ and $Z6$) is the largest, followed by trefoil ($Z10$ and $Z11$), in both IFs. The corresponding more sensitive terms have the same signs and small relative difference between simulation and experimental IFs. For example, $Z6$ is positive in both IFs of ATZ1, and the relative difference is about 10% [$(\mathrm{IFs}_{\mathrm{experimental}} - \mathrm{IFs}_{\mathrm{FEA}})/\mathrm{IFs}_{\mathrm{FEA}}$]. The comparison demonstrates that the two IFs match well.

The compensators (terms of the Zernike polynomials) should be selected to construct sensitivity matrix A. The choice of

Table 1. Parameters of the Mirror

Diameter (mm)	Center Thickness (mm)	Radius of Curvature (mm)	Material	Density (kg/m^3)	Young Modulus (GPa)	Poisson's Ratio
Φ 150	30	560	ULE	2560	96.7	0.25

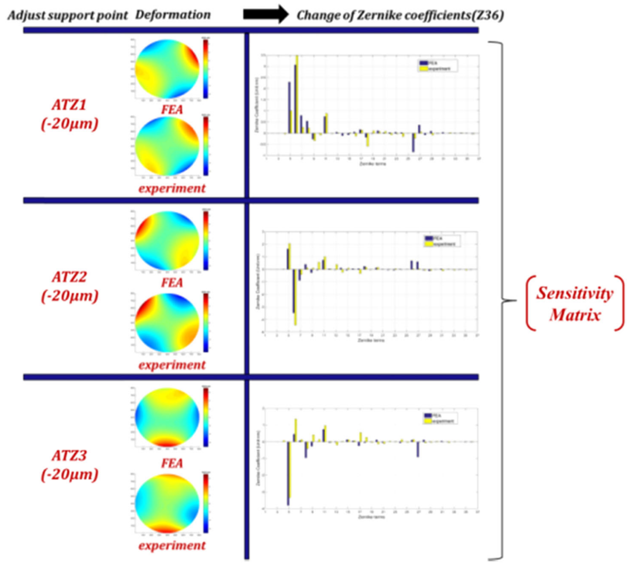

Fig. 4. Experimental and numerical results of IFs.

compensators is determined by two conditions. The first condition is the main surface deformation caused by mounting. As mentioned in Section 2.C, the surface deformation is mainly astigmatism and trefoil, especially the former. The other terms of surface deformation are much smaller. The second condition is the influence functions, which represent the sensitivity. It is easy to get a conclusion from Figure 4 that the astigmatism ($Z5$ and $Z6$) is the most sensitive aberration, followed by trefoil ($Z10$ and $Z11$). It should be noted that $Z10$ and $Z11$ have an azimuthal order of 3, which is the same as adjustable flexure mount. Therefore, it is generally able to correct only one of them separately (either $Z10$ or $Z11$), or change both simultaneously with a linear correlation in sensitivity matrix A.

Considering these conditions, we finally choose $Z5$, $Z6$, and combination of trefoil $k_1 Z10 + k_2 Z11$ as elements of sensitivity matrix A as below. Therefore, we have

$$A = \begin{pmatrix} Z5_{\mathrm{ATZ1}} & Z5_{\mathrm{ATZ2}} & Z5_{\mathrm{ATZ3}} \\ Z6_{\mathrm{ATZ1}} & Z6_{\mathrm{ATZ2}} & Z6_{\mathrm{ATZ3}} \\ k_1 Z10_{\mathrm{ATZ1}} & k_1 Z10_{\mathrm{ATZ2}} & k_1 Z10_{\mathrm{ATZ3}} \\ +k_2 Z11_{\mathrm{ATZ1}} & +k_2 Z11_{\mathrm{ATZ2}} & +k_2 Z11_{\mathrm{ATZ3}} \end{pmatrix},$$

which is a nonsingular matrix, where k_1 and k_2 are constant real numbers and their values depend on the actual situation.

The surface deformation of the compensators and the rest of the Zernike terms is calculated from experimental IFs. Then the ratio of later to former is listed in Table 2. It is clear that the rest of the Zernike terms are much smaller than the compensators. Generally, the surface deformation caused by assembly is several nanometers RMS, and the expected additional surface deformation of other terms during adjustment is smaller than 1 nm RMS.

Table 2. Comparisons of Compensators to Other Terms

	ATZ1	ATZ2	ATZ3
Compensator	1.51 nm RMS	1.51 nm RMS	1.52 nm RMS
Other terms	0.29 nm RMS	0.33 nm RMS	0.31 nm RMS
Ratio	0.19	0.22	0.20

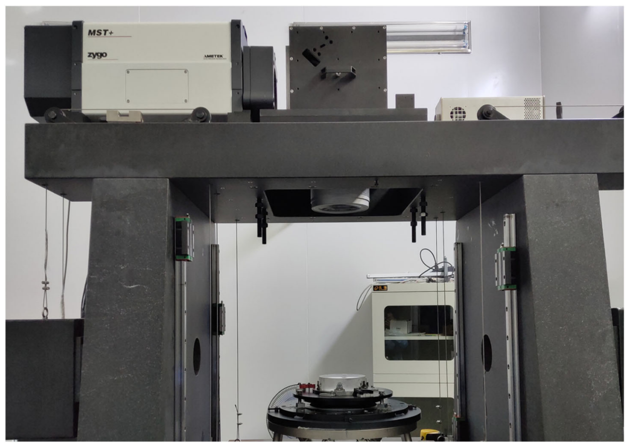

Fig. 5. Experimental device.

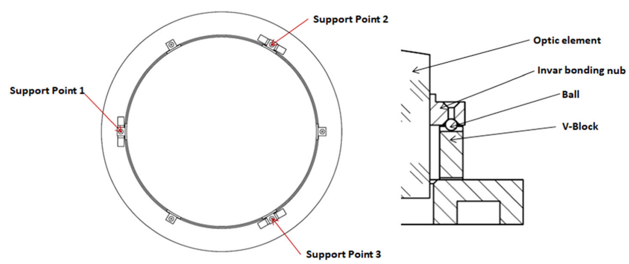

Fig. 6. Schematic diagram of the metrology mount.

4. LABORATORY TEST

A. Experimental Conditions

The surface figure of the optical mirror was measured by a Zygo [20] interferometer. The working surface of the optical mirror is spherical, while the rear surface is a plane. Additionally, the properties of the mirror are listed in Table 1. The experimental setup is shown in Fig. 5.

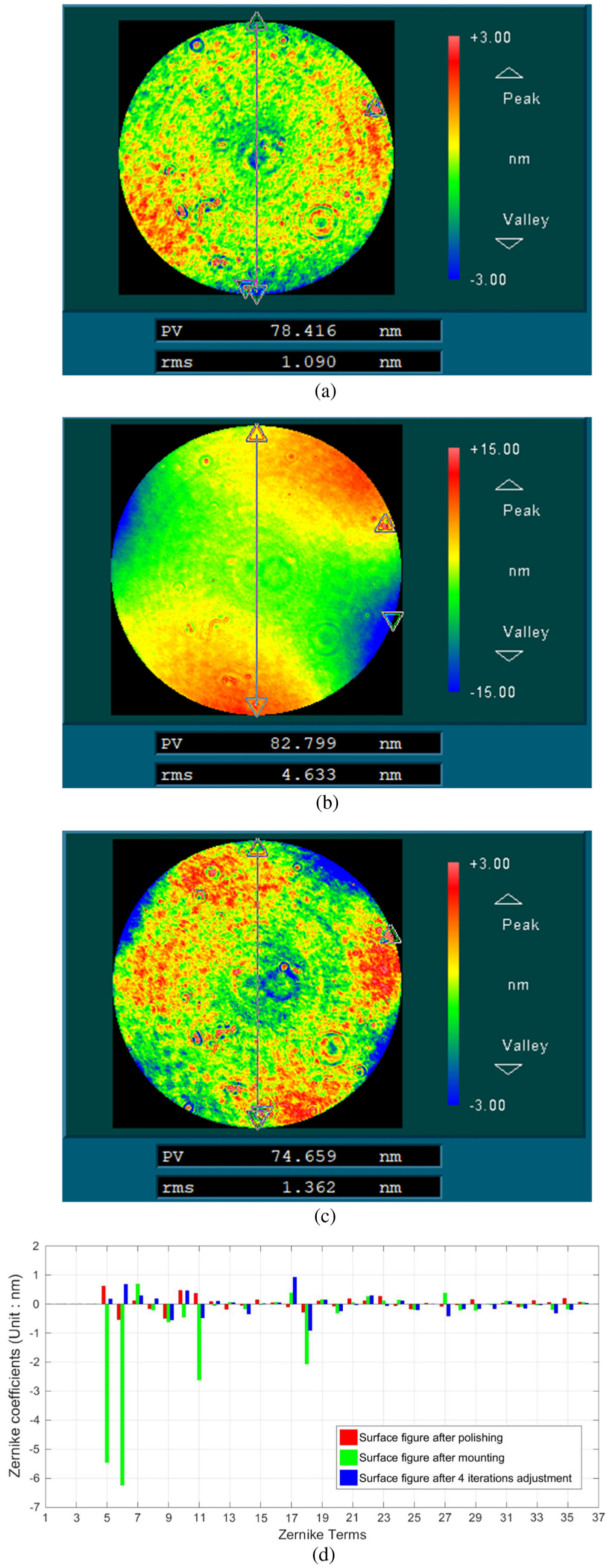

Fig. 7. (a) Surface figure after optical polishing, (b) Zernike coefficients of the surface figure after optical polishing, (c) surface figure before compensation, (d) Zernike coefficients of the surface figure after polishing (red bar), after mounting (green bar), and after four iterations adjustment (blue bar).

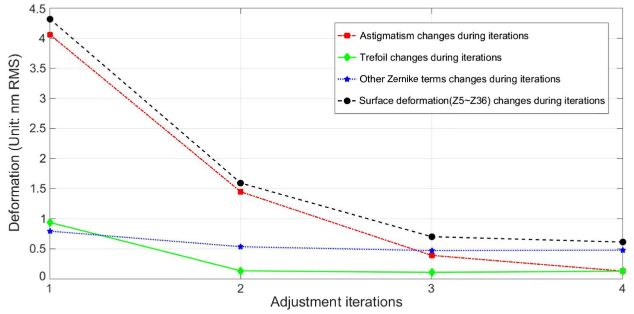

Fig. 8. Surface deformation changes during the iterations.

The interferometer is fixed on the top of measurement frame. The optical axis of the mirror is in a vertical attitude, and the surface under test is upward. The adjustments of three adjustable support points are detected by an inductance meter with 0.1 µm resolution. The experiment was carried out in an ultra-precise environment with ultra-high stability. The temperature of the environment is $22 \pm 0.05°C$, and the vibration isolation level is vibration criterion VC-F. The experimental results verify that the repeatability of measurement is better than 0.1 nm RMS. The first four Zernike terms ($Z1 \sim Z4$) of measurement are closely related to optical mirror position and posture, and they are removed from the measurement results.

B. Compensation for Surface Deformation Using an Adjustable Mount

The surface figure of the tested mirror is 1.1 nm (RMS) after optical polishing, as shown in Fig. 7(a), and its Zernike coefficients are shown by the red bar in Fig. 7(d). Its support for measurement is a metrology mount with high repeatability and reproducibility as shown in Fig. 6.

The optical element and its adjustable flexure mount were assembled. The initial surface shape of the optical element measured by the interferometer is shown in Fig. 7(b) with a surface deformation of 4.6 nm (RMS) after assembly, and the corresponding Zernike coefficients are indicated by the green bar in Fig. 7(d). Experimental sensitivity matrix A was used to obtain the compensation adjustments of the three adjustable support points. Then the adjustments of the adjustable flexure mount are implemented accordingly. The surface deformation is 1.3 nm (RMS) after four iterations, as shown in Fig. 7(c). The blue bar in Fig. 7(d) indicates its Zernike coefficients.

The curves in Fig. 8 represent the surface deformation convergence trend. The red and green curves present astigmatism and trefoil, respectively, during the iterations. The astigmatism and trefoil are significantly reduced at the first adjustment and remain at a very low level in the last iteration. After four iterations, the astigmatism decreases from 4.1 to 0.13 nm RMS, and the trefoil decreases from 0.94 to 0.13 nm RMS. The blue curve shows the rest of the Zernike terms' changes during the iterations. It is slightly decreased. The black curve presents the changes of surface deformation, consisting all Zernike terms in the iterations, which decrease from 4.3 to 0.6 nm RMS.

During the iterations, the residual surface figure (the surface figure after removing the Zernike fitted surface figure, which represents a higher-frequency surface figure) remains the same. The amounts of adjustment of the three adjustable support points are −54.0, 1.9, and −9.4 μm, respectively.

The surface deformation after compensation is slightly larger than that after optical polishing. The main reason is that a small hexafoil error is introduced during mounting structure assembly.

5. CONCLUSION

A mounting structure with the ability to compensate for surface deformation and its method of compensation have been presented. The design and simulation analysis were verified by experiments. In the case of our experimental device, with four iterations of adjustment, the surface deformation of the test mirror has been reduced from 4.6 to 1.3 nm (RMS), which is close to the surface deformation of 1.1 nm (RMS) after optical polishing. Experiments demonstrate that the presented structure and method effectively reduce surface deformation, especially astigmatism and trefoil, caused by the assembly. The adjustable mounting structure performs similarly to an ideal kinematic support and is suitable for optical components with high-precision surface requirements.

Funding. National Science and Technology Major Project (2018ZX02102-002).

REFERENCES AND NOTES

1. L. C. Hale and A. H. Slocum, "Optimal design techniques for kinematic couplings," Precis. Eng. **25**, 114–127 (2001).
2. C. H. Schouten, P. C. J. N. Rosielle, and P. H. J. Schellekens, "Design of a kinematic coupling for precision applications," Precis. Eng. **20**, 46–52 (1997).
3. A. H. Slocum, "Kinematic couplings for precision fixturing—Part I: formulation of design parameters," Precis. Eng. **10**, 85–91 (1988).
4. A. H. Slocum and A. Donmez, "Kinematic couplings for precision fixturing—Part 2: experimental determination of repeatability and stiffness," Precis. Eng. **10**, 115–122 (1988).
5. T. Oversluizen, W. Stoeber, and E. D. Johnson, "Kinematic mounting systems for national synchrotron light source beamlines and experiments," Rev. Sci. Instrum. **63**, 1285–1288 (1992).
6. K. G. Harding, "Flexure mounts for high-resolution optical elements," Proc. SPIE **0959**, 1–19 (1988).
7. H. Kihm and Y. W. Lee, "Optimization and tolerance scheme for a mirror mount design based on optomechanical performance," J. Korean Phys. Soc. **57**, 440–445 (2010).
8. P. Liebetraut, S. Petsch, J. Liebeskind, and H. Zappe, "Elastomeric lenses with tunable astigmatism," Light Sci. Appl. **2**, e98 (2013).
9. J. Reimers, A. Bauer, K. P. Thompson, and J. P. Rolland, "Freeform spectrometer enabling increased compactness," Light Sci. Appl. **6**, e17026 (2017).
10. H. Kihm, H. S. Yang, I. K. Moon, J. H. Yeon, S. H. Lee, and Y. W. Lee, "Adjustable bipod flexures for mounting mirrors in a space telescope," Appl. Opt. **51**, 7776–7783 (2012).
11. M. P. Rimmer and J. C. Wyant, "Evaluation of large aberrations using a lateral-shear interferometer having variable shear," Appl. Opt. **14**, 142–150 (1975).
12. W. Shen, M. Chang, and D. Wan, "Zernike polynomial fitting of lateral shearing interferometry," Opt. Eng. **36**, 905–913 (1997).
13. G. Harbers, P. J. Kunst, and G. W. R. Leibbrandt, "Analysis of lateral shearing interferograms by use of Zernike polynomials," Appl. Opt. **35**, 6162–6172 (1996).
14. G. Leibbrandt, G. Harbers, and P. Kunst, "Wave-front analysis with high accuracy by use of a double-grating lateral shearing interferometer," Appl. Opt. **35**, 6151–6161 (1996).
15. S. De Nicola, P. Ferraro, A. Finizio, G. Pierattini, S. Grilli, I. Gurov, and V. Chugunov, "Wave front aberration analysis in two beam reversal shearing interferometry by elliptical Zernike polynomials," Proc. SPIE **5481**, 27–36 (2004).
16. F. Dai, F. Tang, X. Wang, P. Feng, and O. Sasaki, "Use of numerical orthogonal transformation for the Zernike analysis of lateral shearing interferograms," Opt. Express **20**, 1530–1544 (2012).
17. H. von Brug, "Zernike polynomials as a basis for wave-front fitting in lateral shearing interferometry," Appl. Opt. **36**, 2788–2790 (1997).
18. S. Okuda, T. Nomura, K. Kazuhide, H. Miyashiro, H. Hatsuzo, and K. Yoshikawa, "High precision analysis of lateral shearing interferogram using the integration method and polynomials," Appl. Opt. **39**, 5179–5186 (2000).
19. G.-M. Dai, "Modal wavefront reconstruction with Zernike polynomials and Karhunen-Loève functions," J. Opt. Soc. Am. A **13**, 1218–1225 (1996).
20. Zygo is a registered trademark of Zygo Corporation.